

## Supplementary Discussion

### *Dendritic stratification of RGCs*

The presence of stratified RGC dendrites in *mGluR6-YFP/TeNT* mice may seem surprising, because application of the mGluR6 agonist L-APB (L-2-amino-4-phosphonobutyric acid) was previously reported to prevent dendritic stratification in the developing cat retina<sup>29-31</sup>. In addition, dark rearing in mice was shown to result in an abundance of bistratified RGCs<sup>32</sup>, or an increase in the number of monostatified dendrites laminated near the center of the IPL<sup>33</sup>. However, neither dark rearing in other species<sup>34,35</sup>, nor knock-out of the *mGluR6* gene in mice<sup>36</sup> affected RGC dendritic stratification.

It is important to note that RGC dendrites in mice stratify largely before the onset of light responses<sup>10</sup> when spontaneous activity in the form of retinal waves predominates<sup>37</sup>. We show here that spontaneous glutamate release from ON bipolar cells is reduced in *mGluR6-YFP/TeNT* mice (Fig. 1i - k). By contrast, dark rearing does not influence retinal wave activity in mice<sup>38</sup> and similarly L-APB, while blocking transmission of photoreceptor signals, does not appear to inhibit transmitter release from ON bipolar cell axons during glutamatergic retinal waves<sup>39</sup>. Future studies are therefore needed to determine which aspects of these manipulations account for their effects on stratification and the differences observed between species. In the meantime, our results support a model in which RGC dendritic stratification in mice is guided primarily by the expression of cell adhesion molecules<sup>40,41</sup>.

Recent experiments suggested that following initial stratification, RGC dendrites which laminate close to the center of the IPL, become redistributed towards either the ON or OFF sublamina and that the relative activity of ON and OFF circuits regulates this process<sup>33,42</sup>. While we did not routinely measure the depth within the IPL at which RGC dendrites stratified, in our experiments ON bipolar cell axons and synapses were labeled. This allowed us to ascertain that ON RGCs in *mGluR6-YFP/TeNT* mice were connected overwhelmingly to silenced ON bipolar cells. These findings seem at odds with large-scale activity-dependent redistribution of stratified RGC dendrites.

### *Synaptotropic models of dendrite and axon growth*

Because synapses form at sites of axodendritic contact, the growth of axonal and dendritic arbors during development limits connectivity. The reverse statement, that the extent of synapse formation limits axonal or dendritic growth is less trivial. This latter relationship was first proposed based on fixed tissue studies and is referred to as the synaptotropic model of arbor growth<sup>43</sup>. In recent years, live imaging of axons and dendrites in the zebrafish and tadpole tectum convincingly demonstrated a correlation between the stability of newly formed dendritic and axonal branches and the presence of synapses on those branches<sup>21,44,45</sup>. However, it remains unknown how general a synaptotropic mode of arbor growth is in other systems and if indeed changes in synapse number cause changes in arbor patterns. In the present study we found that in the mouse retina, bipolar cell axons and RGC dendrites form normally when neurotransmission

between them is blocked and the number of synapses is greatly reduced (Fig. 2). A similar dissociation between synaptic density and dendritic patterning was recently reported for cortical pyramidal neurons of NR1 knock-out mice<sup>46</sup>. Moreover, a recent study of *Drosophila* embryos found that dendrites of a central neuron grew further when they received fewer synaptic inputs<sup>47</sup>. Together, these results suggest that the influence of synapses on the patterning of dendritic and axonal arbors may vary widely between different neural circuits.

#### *Multiribbon synapses in mGluR6-YFP/TeNT mice*

Synaptic ribbons are common to sensory neurons that use graded voltage signals and are thought to support continuously varying rates of vesicle fusion to faithfully transmit sensory information<sup>16,48</sup>. At mature ribbon synapses, generally only one ribbon is found per active zone. The signals that restrict the number of ribbons at each synapse remain unknown. Interestingly, hair cells in the developing murine organ of corti show multiribbon synapses before each synapse loses all but one ribbon<sup>49</sup>, whereas bipolar cell terminals in the monkey retina start out with single ribbons<sup>50,51</sup>. We show, that many active zones in silenced bipolar cells of *mGluR6-YFP/TeNT* mice accumulate multiple ribbons (Fig.3). We argue that since the TeNT-substrate VAMP2 is neither a component of Piccolo-Bassoon transport vesicles nor precursor spheres<sup>17,18,52</sup> from which active zones and ribbons are assembled, this is unlikely to be a direct effect of TeNT. One could reason that the reduced number of active zones in TeNT-expressing bipolar cells causes synaptic ribbons to accumulate. However, if there were no rule other than matching numbers of active zones and synaptic ribbons, multiribbon synapses and empty active zones should be frequently encountered in wildtype retinas. Because neither we (Fig. 3 and Supplementary Figs. 7 and 8) nor others<sup>50,51,53-58</sup> ever observed multiribbon synapses in wildtype bipolar cells, we propose instead that TeNT by blocking transmitter release interferes with a feedback signal that normally restricts ribbon placement at active zones. Future experiments are needed to test this hypothesis.

Finally, does the accumulation of ribbons at fewer active zones cause the reduced number of synapses? The developmental timeline argues against such a link. We observed drastic differences in bipolar cell - RGC synaptogenesis at P9 several days before the appearance of synaptic ribbons in bipolar cell terminals<sup>57</sup>.

## Supplementary Figures and Legends

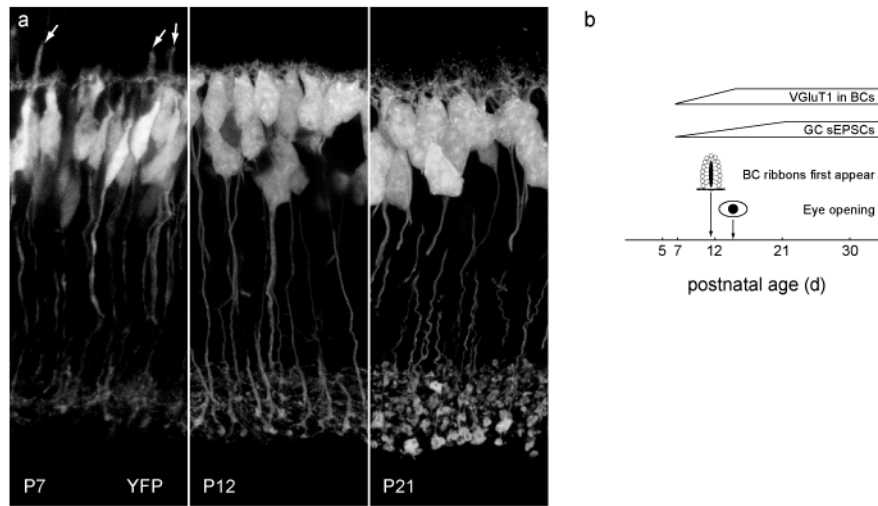


**Figure S1 | Transgene in *mGluR6-YFP/TeNT* mice is expressed throughout the period of functional bipolar cell - RGC circuit assembly. a**, Vibratome sections through retinas of *mGluR6-YFP/TeNT* mice at the indicated postnatal ages. YFP signal shows transgene expression in ON bipolar cells at least from P7, when bipolar cells are starting to elaborate axonal side branches and still retract neuroepithelial-like processes (arrows), to P21 when bipolar cell morphology is mature<sup>14</sup>. **b**, Timeline of bipolar cell - RGC circuit development. sEPSCs can first be recorded from RGCs at P7<sup>19,59</sup>, when VGLuT1 starts being expressed in bipolar cell terminals<sup>19,60</sup>. Thus, the transgene in *mGluR6-YFP/TeNT* mice is expressed at least from the normal developmental onset of bipolar cell glutamate release and precedes the assembly of synaptic ribbons and eye opening by several days<sup>57</sup>.

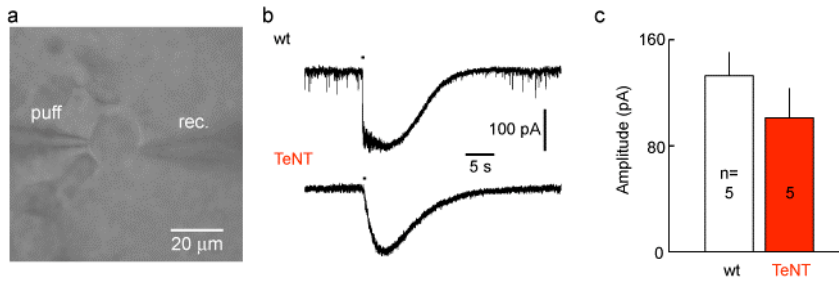


**Figure S2 | Focal application of kainate elicits excitatory currents in ON RGCs of wildtype and *mGluR6-YFP/TeNT* mice.** **a**, Representative bright field image of a patch-clamp recording from an ON RGC in a flat mount preparation. Recording electrode is shown on the right (rec.). Kainate (100 μM) was pressure applied (20 psi, 300 ms) from a second electrode (puff) positioned next to the soma of the recorded cell. **b**, Representative traces of currents elicited by kainate application onto ON RGCs from wildtype (upper trace) and *mGluR6-YFP/TeNT* (lower trace) mice at P21. Cells were held at -60 mV (i.e. the reversal potential for chloride currents in our recording conditions) to isolate excitatory currents. Note the absence of spontaneous EPSCs in the baseline of the recording from the ON RGC in *mGluR6-YFP/TeNT* compared to wildtype background. **c**, Summary data (mean ± s.e.m.) of the amplitude of EPSCs elicited by application of kainate (n = 5 cells for both wildtype and *mGluR6-YFP/TeNT*). For each cell, kainate was applied four times and the average amplitude used in the summary data.

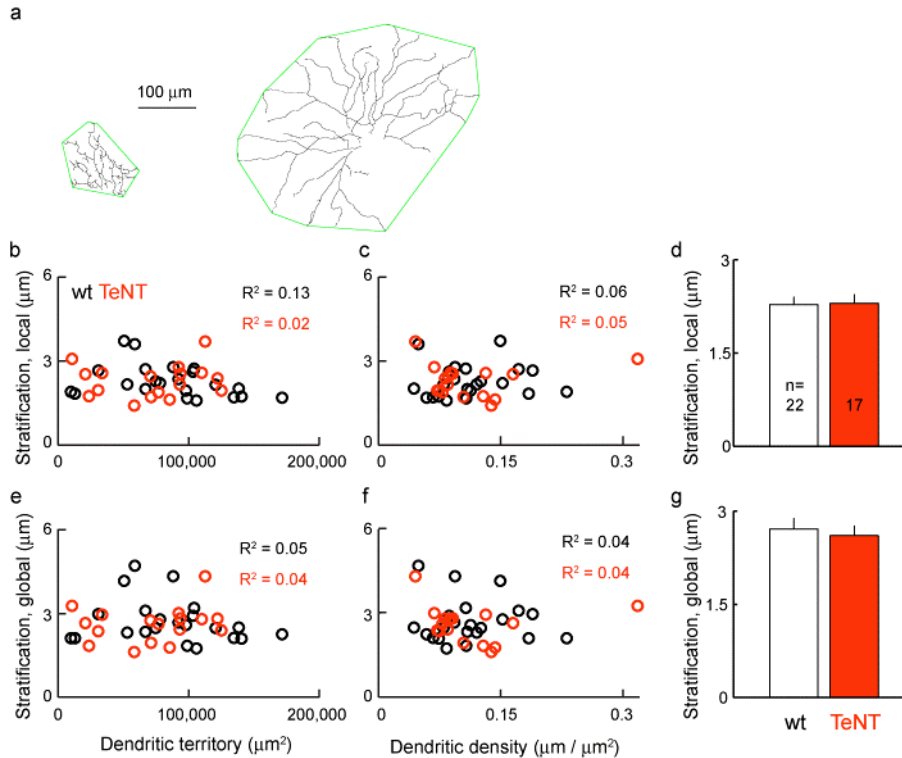


**Figure S3 | Stratification of dendrites from a wide range of RGC types appears unchanged in *mGluR6-YFP/TeNT* compared to wildtype mice.** **a**, Skeletonized dendritic arbors of two representative ON RGCs in *mGluR6-YFP/TeNT* background. The dendritic territory of an RGC was defined as the area of the smallest convex polygon (green lines) to encompass all of the dendrite in a z-projection. **b - g**, Dendritic skeletons consisted of  $\sim 0.5 \mu\text{m}$  long connected segments. Stratification was measured as the standard deviation (s.d.) of the z-position of those segments. To avoid primary processes, segments within  $10 \mu\text{m}$  from the soma were excluded from the analysis. When calculating the local stratification index (**b - d**) for each segment the average z-position used in the calculation of the s.d. was the average z-position of segments within  $30 \mu\text{m}$  in x-y of the current segment. This reduced the potential influence of irregularities in the tissue. Note however, that none of our conclusions depend on this restriction and a global stratification index (**e - g**), i.e. the s.d. calculated using the average z-position of all segments, gave qualitatively similar results. **b, c**, Stratification (local index) was not significantly correlated with dendritic territory (**b**) or density (**c**), two of the three parameters found most useful in separating RGC types<sup>61</sup>, and appeared to be narrowly confined without apparent outlying clusters, in wildtype and *mGluR6-YFP/TeNT* mice. These results suggest that as observed previously, different types of monostратified ON RGCs had similar stratification width<sup>61</sup>, and that stratification for a wide range of ON RGC types was unaffected by blockade of input activity from ON bipolar cells in *mGluR6-YFP/TeNT* mice. **d**, Summary data (mean  $\pm$  s.e.m) for local stratification index of ON RGCs. **e - g**, same as **b - d** but using global instead of local stratification index. Note that the data set used in this figure is not overlapping with that of Fig. 2, and was acquired using a 25x 0.8NA oil instead of a 60x 1.35NA oil objective to allow us to capture the whole dendritic tree of the largest cells in a single stack.

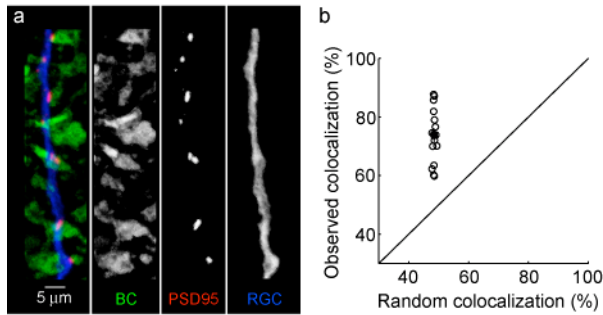


**Figure S4 | PSD95-CFP puncta are localized opposite silenced bipolar cell terminals in *mGluR6-YFP/TeNT* mice.** **a**, Representative dendritic branch (tdTomato, blue) of a ON RGC from a *mGluR6-YFP/TeNT* mouse (P21) showing the apposition of PSD95-CFP puncta (red) and presynaptic terminals (YFP, green). **b**, Sixteen RGCs with a total of 10,982 PSD95-CFP puncta were evaluated for colocalization of presynaptic (YFP) and postsynaptic (PSD95-CFP) labels in *mGluR6-YFP/TeNT* mice. Significance was assessed by comparing the colocalization calculated for the observed PSD95-CFP puncta (Observed colocalization) with the colocalization measured when puncta were randomly repositioned along the dendritic arbor in a Monte Carlo simulation (Random Colocalization) as described previously<sup>13</sup>. For all of the 16 cells (open circles) tested in this way  $p < 0.01$ . Mean ( $\pm$  s.e.m.) for this group of cells is shown by the filled circle (errorbars). These results together with previous studies support the use of PSD95 as a marker of bipolar cell - RGC synapses in the retina<sup>13,62,63</sup>.

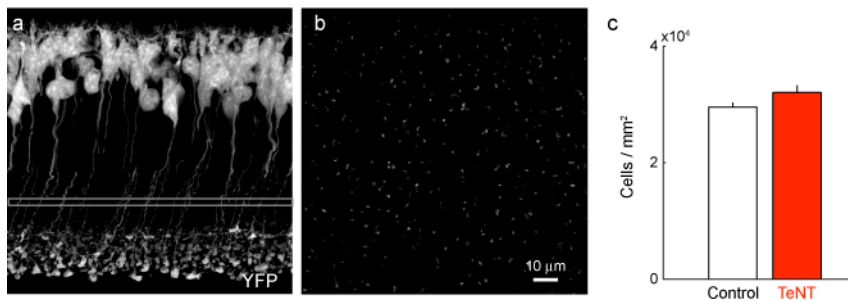


**Figure S5 | The density of ON bipolar cells is unaffected in *mGluR6-YFP/TeNT* mice.** **a**, Vibratome section through an *mGluR6-YFP/TeNT* retina. The gray box indicates the approximate level at which two photon images were taken in retinal flat mounts for counting of axon stalks. **b**, Two photon image acquired roughly at the level indicated in **a** in the retina of an *mGluR6-YFP/TeNT* mouse. Bipolar cell number was determined using custom written software to threshold the image, identify connected pixels in the thresholded image as objects and count them. **c**, Summary data (mean  $\pm$  s.e.m.) comparing bipolar cell densities measured in *mGluR6-GFP*<sup>14</sup> (control) and *mGluR6-YFP/TeNT* mice (TeNT).  $n = 2$  mice per genotype and 4 regions of interest per mouse.

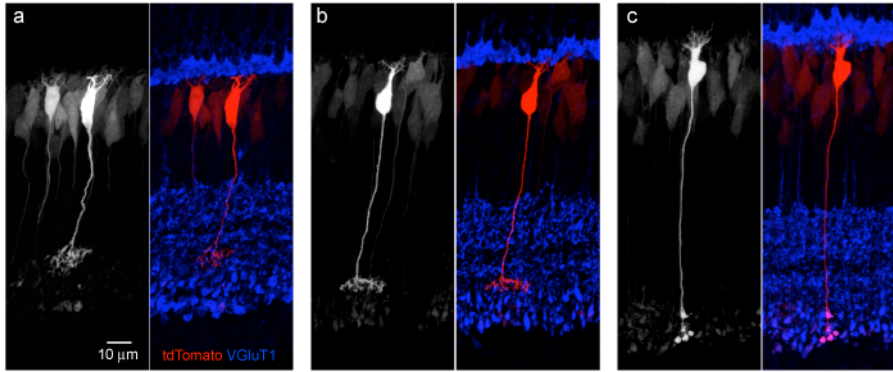


**Figure S6 | Isolated type 6 and 7 ON cone bipolar cells and rod bipolar are brightly labeled in *mGluR6-tdTomato* mice.** **a-c**, Vibratome sections through a P21 retina of an *mGluR6-tdTomato* mouse showing representative type 6 (**a**) and type 7 (**b**) ON cone bipolar cells as well as a rod bipolar cells (**c**). Isolated bipolar cells in this mouse line show bright tdTomato fluorescence (*left panels*). For reference, all bipolar cell terminals in the IPL were labeled with anti-VGluT1 (*right panels*).

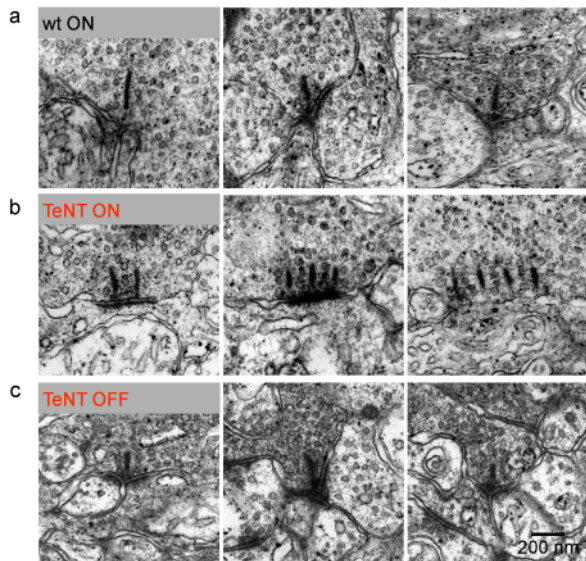


**Figure S7 | Multiple ribbons at synapses of ON bipolar cell terminals in *mGluR6-YFP/TeNT* mice.** **a-b**, Electron micrographs of representative ON bipolar cell terminals in P21 wildtype (**a**) and *mGluR6-YFP/TeNT* retinas (**b**). **c**, Electron micrographs of representative OFF bipolar cell terminals in a retina of a P21 *mGluR6-YFP/TeNT* mouse.

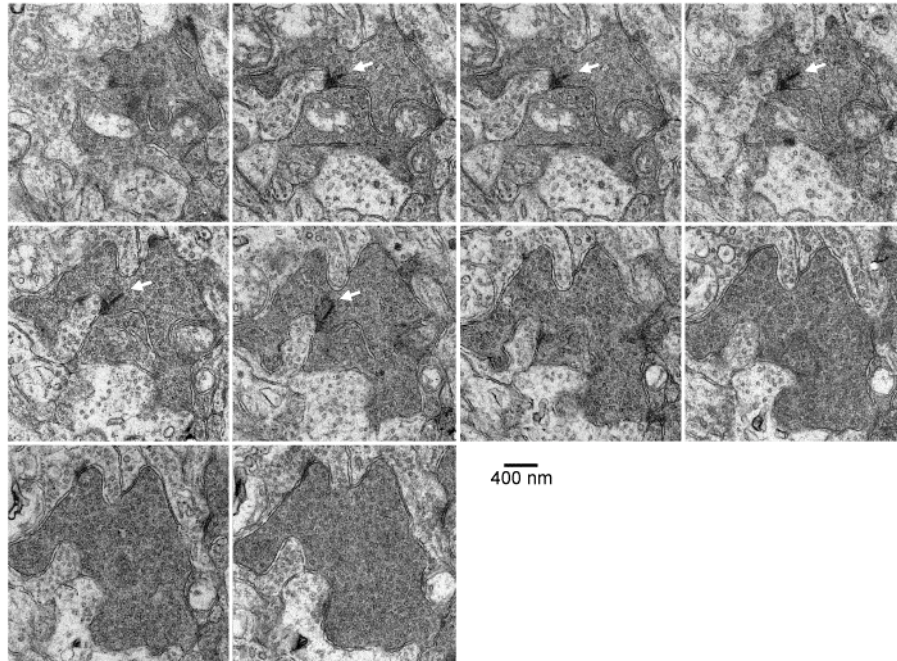


**Figure S8 | Serial section electron microscopy confirms that wildtype bipolar cell active zones contain single ribbons.** Consecutive 70 nm sections through a representative rod bipolar cell terminal showing a single ribbon (arrow) at an active zone. We never found multiple ribbons at active zones of wildtype bipolar cells. Together with many other studies in a variety of species that likewise always observed isolated ribbons at bipolar cell active zones during development and at maturity<sup>50,51,53-58</sup> this suggests that accumulation of multiple ribbons is unique to *mGluR6-YFP/TeNT* mice.

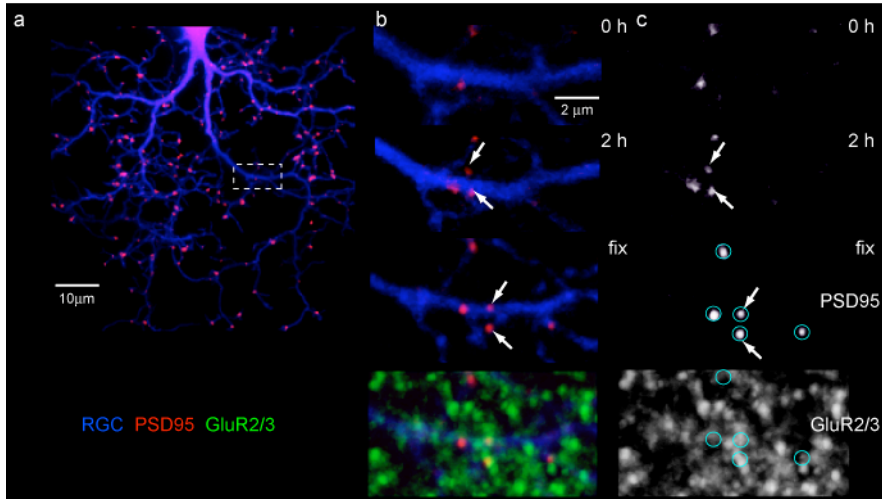


**Figure S9 | Posthoc immunostaining reveals the presence of glutamate receptors at newly formed PSD95 clusters.** **a**, First of two time points of an image series showing the dendritic arbor of a P9 RGC labeled with td-Tomato (blue) and glutamatergic postsynaptic densities labeled with PSD95-CFP (red). **b**, Time series of the region indicated by the white box in **a** in which two new PSD95 clusters appeared (arrows). The retina was fixed 30 minutes after the second time point and labeled with anti-GluR2/3 (green) receptor subunits. Post-fixation images with and without the antibody signal are shown in the bottom two panels (fix) **c**, PSD95-CFP signal (top three panels) of time lapse and post-fixation images is shown in isolation, followed by the isolated anti-GluR2/3 signal (bottom panel). The position of PSD95-CFP clusters in the post-fixation image is indicated by cyan circles. Colocalization of anti-GluR2/3 staining PSD95-CFP signal was found at all (9/9) newly formed synapses analyzed in this way.

## Supplementary Notes

- 29 Bisti, S., Gargini, C. & Chalupa, L. M. Blockade of glutamate-mediated activity in the developing retina perturbs the functional segregation of ON and OFF pathways. *J. Neurosci.* **18**, 5019-5025 (1998).
- 30 Bodnarenko, S. R. & Chalupa, L. M. Stratification of ON and OFF ganglion cell dendrites depends on glutamate-mediated afferent activity in the developing retina. *Nature* **364**, 144-146 (1993).
- 31 Bodnarenko, S. R., Jeyarasasingam, G. & Chalupa, L. M. Development and regulation of dendritic stratification in retinal ganglion cells by glutamate-mediated afferent activity. *J. Neurosci.* **15**, 7037-7045 (1995).
- 32 Tian, N. & Copenhagen, D. R. Visual stimulation is required for refinement of ON and OFF pathways in postnatal retina. *Neuron* **39**, 85-96 (2003).
- 33 Xu, H. P. & Tian, N. Retinal ganglion cell dendrites undergo a visual activity-dependent redistribution after eye opening. *J. Comp. Neurol.* **503**, 244-259 (2007).
- 34 Leventhal, A. G. & Hirsch, H. V. Effects of visual deprivation upon the morphology of retinal ganglion cells projecting to the dorsal lateral geniculate nucleus of the cat. *J. Neurosci.* **3**, 332-344 (1983).
- 35 Lau, K. C., So, K. F. & Tay, D. Effects of visual or light deprivation on the morphology, and the elimination of the transient features during development, of type I retinal ganglion cells in hamsters. *J. Comp. Neurol.* **300**, 583-592 (1990).
- 36 Tagawa, Y., Sawai, H., Ueda, Y., Tauchi, M. & Nakanishi, S. Immunohistological studies of metabotropic glutamate receptor subtype 6-deficient mice show no abnormality of retinal cell organization and ganglion cell maturation. *J. Neurosci.* **19**, 2568-2579 (1999).
- 37 Wong, R. O. Retinal waves and visual system development. *Annu. Rev. Neurosci.* **22**, 29-47 (1999).
- 38 Demas, J., Eglén, S. J. & Wong, R. O. Developmental loss of synchronous spontaneous activity in the mouse retina is independent of visual experience. *J. Neurosci.* **23**, 2851-2860 (2003).
- 39 Kerschensteiner, D. & Wong, R. O. A precisely timed asynchronous pattern of ON and OFF retinal ganglion cell activity during propagation of retinal waves. *Neuron* **58**, 851-858 (2008).
- 40 Yamagata, M., Weiner, J. A. & Sanes, J. R. Sidekicks: synaptic adhesion molecules that promote lamina-specific connectivity in the retina. *Cell* **110**, 649-660 (2002).
- 41 Yamagata, M. & Sanes, J. R. Dscam and Sidekick proteins direct lamina-specific synaptic connections in vertebrate retina. *Nature* **451**, 465-469 (2008).
- 42 Xu, H. P. & Tian, N. Glycine receptor-mediated synaptic transmission regulates the maturation of ganglion cell synaptic connectivity. *J. Comp. Neurol.* **509**, 53-71 (2008).
- 43 Vaughn, J. E. Fine structure of synaptogenesis in the vertebrate central nervous system. *Synapse* **3**, 255-285 (1989).
- 44 Meyer, M. P. & Smith, S. J. Evidence from in vivo imaging that synaptogenesis guides the growth and branching of axonal arbors by two distinct mechanisms. *J. Neurosci.* **26**, 3604-3614 (2006).

- 45 Ruthazer, E. S., Li, J. & Cline, H. T. Stabilization of axon branch dynamics by  
synaptic maturation. *J. Neurosci.* **26**, 3594-3603 (2006).
- 46 Ultanir, S. K. et al. Regulation of spine morphology and spine density by NMDA  
receptor signaling in vivo. *Proc. Natl. Acad. Sci. U S A* **104**, 19553-19558 (2007).
- 47 Tripodi, M., Evers, J. F., Mauss, A., Bate, M. & Landgraf, M. Structural  
homeostasis: compensatory adjustments of dendritic arbor geometry in response  
to variations of synaptic input. *PLoS Biol.* **6**, e260 (2008).
- 48 Lagnado, L. Ribbon synapses. *Curr. Biol.* **13**, R631 (2003).
- 49 Sobkowicz, H. M., Rose, J. E., Scott, G. E. & Slapnick, S. M. Ribbon synapses in  
the developing intact and cultured organ of Corti in the mouse. *J. Neurosci.* **2**,  
942-957 (1982).
- 50 Nishimura, Y. & Rakic, P. Development of the rhesus monkey retina: II. A three-  
dimensional analysis of the sequences of synaptic combinations in the inner  
plexiform layer. *J. Comp. Neurol.* **262**, 290-313 (1987).
- 51 Nishimura, Y. & Rakic, P. Development of the rhesus monkey retina. I.  
Emergence of the inner plexiform layer and its synapses. *J. Comp. Neurol.* **241**,  
420-434 (1985).
- 52 Ziv, N. E. & Garner, C. C. Cellular and molecular mechanisms of presynaptic  
assembly. *Nat. Rev. Neurosci.* **5**, 385-399 (2004).
- 53 McGuire, B. A., Stevens, J. K. & Sterling, P. Microcircuitry of bipolar cells in cat  
retina. *J. Neurosci.* **4**, 2920-2938 (1984).
- 54 Tsukamoto, Y., Morigiwa, K., Ueda, M. & Sterling, P. Microcircuits for night  
vision in mouse retina. *J. Neurosci.* **21**, 8616-8623 (2001).
- 55 Dowling, J. E. & Boycott, B. B. Organization of the primate retina: electron  
microscopy. *Proc. R. Soc. Lond. B. Biol. Sci.* **166**, 80-111 (1966).
- 56 Maslim, J. & Stone, J. Synaptogenesis in the retina of the cat. *Brain Res.* **373**, 35-  
48 (1986).
- 57 Fisher, L. J. Development of synaptic arrays in the inner plexiform layer of  
neonatal mouse retina. *J. Comp. Neurol.* **187**, 359-372 (1979).
- 58 Crooks, J. & Morrison, J. D. Synapses of the inner plexiform layer of the area  
centralis of kitten retina during postnatal development: a quantitative study. *J.*  
*Anat.* **163**, 33-47 (1989).
- 59 Tian, N. & Copenhagen, D. R. Visual deprivation alters development of synaptic  
function in inner retina after eye opening. *Neuron* **32**, 439-449 (2001).
- 60 Sherry, D. M., Wang, M. M., Bates, J. & Frishman, L. J. Expression of vesicular  
glutamate transporter 1 in the mouse retina reveals temporal ordering in  
development of rod vs. cone and ON vs. OFF circuits. *J. Comp. Neurol.* **465**, 480-  
498 (2003).
- 61 Kong, J. H., Fish, D. R., Rockhill, R. L. & Masland, R. H. Diversity of ganglion  
cells in the mouse retina: unsupervised morphological classification and its limits.  
*J. Comp. Neurol.* **489**, 293-310 (2005).
- 62 Koulen, P., Fletcher, E. L., Craven, S. E., Brecht, D. S. & Wassle, H.  
Immunocytochemical localization of the postsynaptic density protein PSD-95 in  
the mammalian retina. *J. Neurosci.* **18**, 10136-10149 (1998).

- <sup>63</sup> Jakobs, T. C., Koizumi, A. & Masland, R. H. The spatial distribution of glutamatergic inputs to dendrites of retinal ganglion cells. *J. Comp. Neurol.* **510**, 221-236 (2008).